IEEE Photonics Journal
An IEEE Photonics Society Publication

Open Access

Broadband Antireflection Coatings Made of Resonant Submicron- and Micron-Sized SiGe Particles Grown on Si Substrates

Volume 13, Number 3, June 2021

Alexander A. Shklyaev
Andrei V. Tsarev

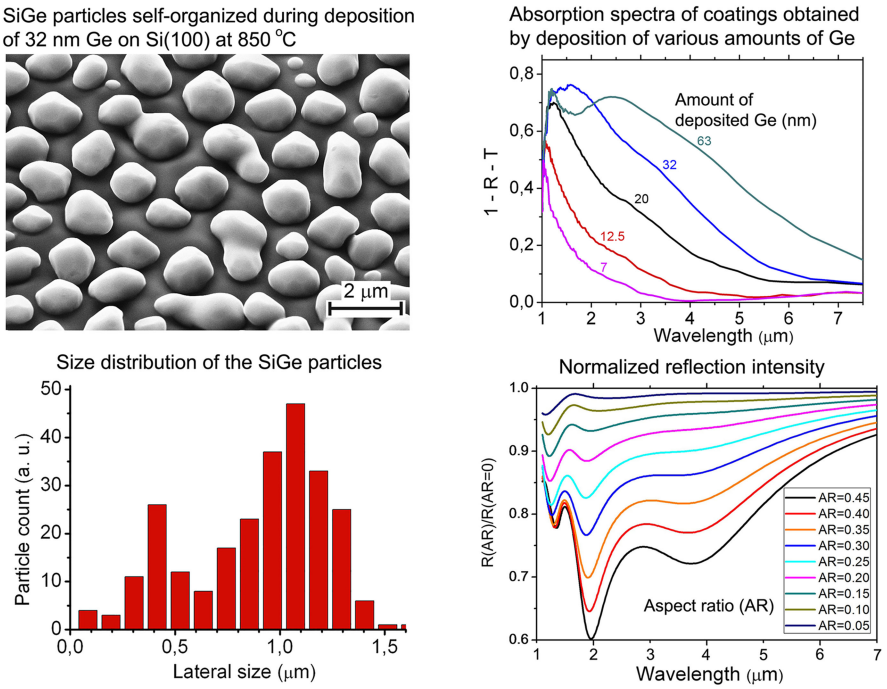

DOI: 10.1109/JPHOT.2021.3081100

Broadband Antireflection Coatings Made of Resonant Submicron- and Micron-Sized SiGe Particles Grown on Si Substrates

Alexander A. Shklyaev [1,2] **and Andrei V. Tsarev** [1,2]

[1]Novosibirsk State University, Novosibirsk 630090, Russia
[2]A.V. Rzhanov Institute of Semiconductor Physics, Novosibirsk 630090, Russia

DOI:10.1109/JPHOT.2021.3081100

Manuscript received April 20, 2021; accepted May 12, 2021. Date of publication May 18, 2021; date of current version June 3, 2021. This work was supported by Ministry of Science and Higher Education of the Russian Federation under Grant 075-15-2020-797 (13.1902.21.0024)) Corresponding author: Alexander A. Shklyaev (e-mail: shklyaev@isp.nsc.ru).

Abstract: The solid-state dewetting phenomenon was used to obtain submicron- and micron-sized SiGe particle arrays by the Ge deposition on Si(100) substrates. Their transmission and reflection spectra were measured and numerically modeled by the FDTD method. They exhibit resonance effects in broad infrared spectral ranges, depending on the particle size. The broadband antireflection property is associated with wide particle size distributions and the influence of a high-index substrate. The results show that the dewetting phenomenon provides the natural formation of arrays of particles shaped as close to a sphere segment, and they turned out to be effective as antireflection coatings.

Index Terms: Thin film coatings, optical properties of photonic materials, metamaterials, fabrication and characterization, numerical simulation, FDTD method.

1. Introduction

The use of antireflection coatings essentially improves the efficiency of various optoelectronic devices, in particular, photodetectors. Coatings generating optical resonances have recently been introduced for this purpose [1]–[4]. The simplest ones, from the technological viewpoint of their fabrication, are coatings of a thin metal perforated film containing gratings of subwavelength-sized holes. When electromagnetic (EM) radiation interacts with them in the mid-IR region, it can cause the EM wave leakage through the holes due to the surface plasmon excitation leading to a local concentration of electromagnetic waves in the substrate surface layers [1]–[3], [5], [6]. This effect can be enhanced by means of the Rayleigh anomaly introducing a diffraction effect occurring owing to the EM radiation scattering on the hole edges [6]–[8]. It was shown that the placement of dielectric particles into metal film holes can give an additional positive effect based on the excitation of magnetic and electrical resonances in dielectric particles [2], [4], [9]–[11]. Although the use of such hybrid metal-dielectric antireflection coatings provides a significant increase in the efficiency of optoelectronic converters in the mid-IR region, they have the disadvantage of containing metal components that cause the dissipation of EM radiation. The implementation of all-dielectric antireflection coatings could significantly reduce this undesirable effect.

New features of optical properties continue to be revealed in metasurfaces consisting of dielectric particle arrays [12], [13]. Particles made of Si-based materials are of particular interest due to their wide commercial applications and advanced microelectronic technology. An important aspect is that the refractive index (n) of Si is relatively high, due to which optical resonances appear in Si particles at EM wavelengths several times smaller than the particle size [10], [11]. Ge has n greater than that of Si. The use of Ge and SiGe instead of Si allows reducing the particle size in order to obtain optical resonances at the same wavelengths. In addition, particles with higher n are characterized by greater resonance Q-factors [11], [14]–[16].

Several methods for obtaining dielectric particle arrays, among which there are approaches using various lithographic techniques [17]–[20] and laser ablation [21], [22], are being developed. The most technologically simple approaches are based on the self-organization of continuous surface layers through their agglomeration into compact particles by means of the dewetting phenomenon. This phenomenon was best studied for Si [23]–[29] and Ge [24], [30]–[32] layers on SiO_2. The solid-state dewetting phenomenon has recently been observed for Ge layers on Si substrates [33], [34]. As in the case of Si and Ge layers on SiO_2, the Ge dewetting from Si can be realized both by the high temperature annealing of continuous Ge layers initially deposited on Si substrates at relatively low temperatures [35], [36] and during the Ge deposition on Si substrates directly at high temperatures ($\geq$750 °C) [34], [37].

The strong effect on the reflection and transmission of EM radiation caused by coatings consisting of dielectric particles originates from the destructive interference with resonant magnetic and electric dipole modes. The minimum reflection and transmission appears at the wavelengths at which the EM fields of magnetic and electric dipole modes are equal in magnitude [16], [38]–[42]. Depending on the shape of particles and their concentration and spatial distribution, zero intensity of reflected and transmitted EM radiation can be obtained. The spectral position of the dipole modes relative to each other depends, in particular, on the particle shape. For particles shaped as a disk, which is described by two parameters: diameter (d) and height (h), the spectral position of dipole modes relative to each other is determined by the aspect ratio (AR) value, AR $= h/d$. The spectral positions of dipole modes have different dependences on AR. Calculations have shown that the positions of dipole modes coincide for disk-shaped particles with AR $\sim$0.4–0.5 [34], [40], [43]. Such AR values are often observed in particles formed using various methods [35]–[37], in particular, by the agglomeration of continuous layers on non-wettable surfaces [18], [20], [23], [38], [39]. Particles with such AR also predominantly formed during the Ge deposition on Si(100) [34], [37], [49].

In this work, the dewetting phenomenon was used to form coatings of SiGe particles with sizes from submicron to micron, depending on the amount of Ge deposited on Si(100) substrates. The reflection and transmission spectra were measured in the wavelength range from $\sim$1 to 16 μm. They show the presence of strong effects from the resonant interaction of EM radiation with SiGe particle arrays. The dependence of reflection and transmission minima on the particle size distribution was obtained. It is found that, in the presence of a wide particle size distribution, the resonant EM modes of smaller particles produce a stronger contribution to the destructive interference with incident EM radiation than that of larger particles. It is suggested that the observed broadband antireflection property of coatings consisting of SiGe particles is associated with a rather wide particle size distribution in combination with the resonance mode broadening of individual particles [50], which occurs due to the influence of high-index substrates. The results of our numerical simulation using the FDTD method confirmed the broadband properties of the SiGe particle on Si substrates due to the strong EM resonances in particles with relative large AR values of about 0.4, despite their low Q-factor.

2. Experimental Details

The experiments on the Ge growth were carried out in an ultrahigh-vacuum chamber with a base pressure of about 1×10^{-10} Torr manufactured by Omicron. Samples ($10 \times 2 \times 0.3$ mm^3) cut from n-type Si(100) wafers were used as substrates. Clean Si surfaces of the substrates were

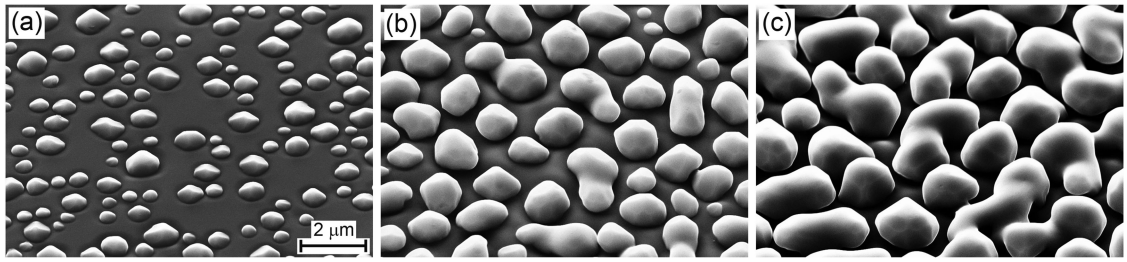

Fig. 1. (a–c) SEM images of the samples obtained after the Ge deposition on Si(100) at 850 °C in the amounts of 7, 32 and 63 nm, respectively. Images are taken at about a 45° electron beam incidence relative to the sample surface. The scale bar for the images is shown in (a).

prepared by the flash direct-current heating at 1250–1300 °C. A Knudsen cell with a BN crucible was used for the Ge deposition at the rate up to 1.0 nm/min, as was described elsewhere [49]. To calibrate the Ge deposition rate as a function of Knudsen cell temperature, relatively thick Ge films (∼100 nm) were deposited on Si substrates at about room temperature. The film thickness was measured using the scanning electron microscope (SEM) images of the sample cross-sections. The coatings with SiGe particles were obtained by the Ge deposition on the Si(100) samples at the temperature of 850 °C. The sample temperature was measured using an IMPAC IGA 12 pyrometer. After the sample removal from the growth chamber, their surface morphology was examined with a Pioneer SEM manufactured by Raith, and the surface chemical composition was determined with energy-dispersive X-ray spectroscopy. The reflection and transmission spectra were measured by a Simex Fourier transform infrared spectrometer FT-801 operating in the range from 1 to 20 μm. The transmission spectra were obtained under normal incidence. To measure the reflectance, the angle of an EM beam incidence was 45 degrees, and the reflected EM radiation was collected within a solid angle of about 45 degrees. Air was used as the reference for measuring the transmittance, and a gold film deposited on a polished Si wafer was used as a reference for measuring the reflectance. The incidence angle of 45 degrees in the reflectance measurement was used for convenience. Spinelli et al. [50] showed that the reflectance from arrays of compact particles in the spectral region of magnetic and electrical resonances is almost independent of the incidence angle.

3. Results and Discussion

3.1 Characterization of the Coatings with SiGe Particles on Si(100)

The Ge deposition on Si(100) at 850 °C leads to the formation of compact three-dimensional particles [34]. It was shown that, due to a strong intermixing of Si and Ge atoms at the SiGe/Si(100) interface, the particles have the composition Si_xGe_{1-x} with x from ∼0.8 to 0.9 depending on the deposited Ge amount and the Ge deposition rate [37], [49]. The SiGe particles had a sharp compositional boundary with the Si(100) substrate and large contact angles with the substrate [37]. This indicates that the SiGe layers do not wet the Si surface, despite the strong intermixing of Ge and Si atoms at the SiGe/Si(100) interface [37], [49]. The SiGe particle size increases with the deposited Ge amount. At the same time, the particle concentration decreases due to coalescence of nearby particles, but they remain compact (Fig. 1) due to the intense diffusion and dewetting of Si by SiGe.

For relatively small amounts of deposited Ge, the SiGe particles are formed only due to the nucleation at the initial Ge deposition stage. As a function of their size, they form the monomodal distribution (Fig. 2(a)). As the deposited Ge amount increases, they grow in size so that closely spaced particles coalesce to form relatively large compact particles. This results in a significant broadening of the particle size distribution (Fig. 2(b)). With the further increase in the deposited Ge amount, large particles obtained by coalescence are characterized by a separate peak in the size distribution (Fig. 2(c)), and the distribution becomes bimodal. Lager amounts of deposited Ge lead

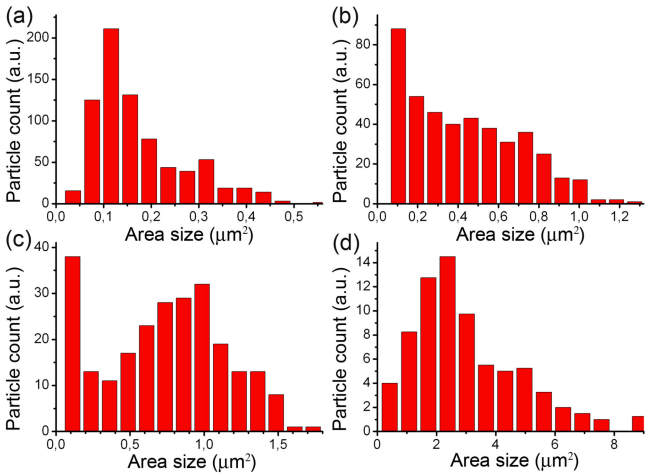

Fig. 2. (a–d) The SiGe particle concentration as a function of a surface area occupied by an island for the samples obtained by the Ge deposition in the amount of 7, 20, 32 and 63 nm on Si(100) at 850 °C, respectively.

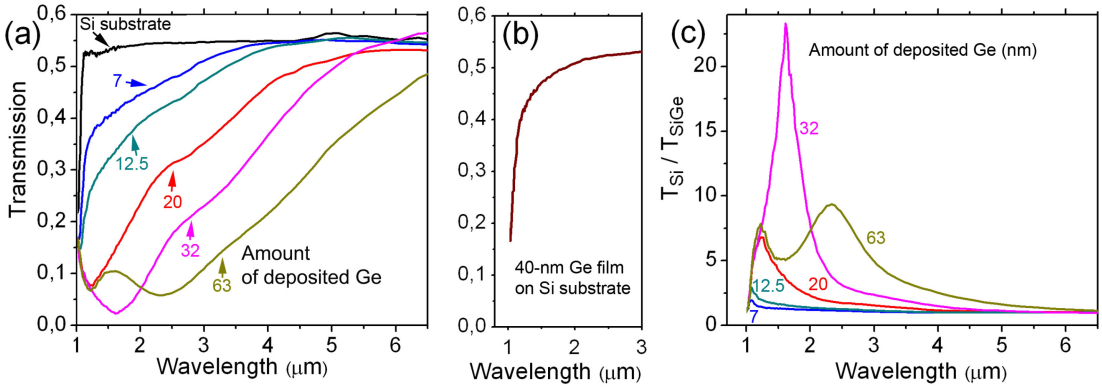

Fig. 3. Transmission spectra of (a) a Si(100) substrate and the samples prepared by the Ge deposition in the amount of 7, 12.5, 20, 32 and 63 nm on Si(100) at 850 °C, as marked in (a), and (b) the Si(100) substrate covered with the 40 nm continuous Ge film deposited at room temperature. (c) Wavelength dependences of the ratio of the transmission spectra (shown in (a)) of Si(100) substrates coated with SiGe particles to the transmission spectrum of the uncoated Si(100) substrate.

to a further decrease in the concentration of particles not involved in the coalescence, and the size distribution, again, becomes monomodal (Fig. 2(d)).

3.2 Optical Properties

The transmission spectra (T_{SiGe}) of the samples coated with SiGe particles show a strong dependence on the particle size (Fig. 3(a)). With an increase in the particle size, the transmission minimum shifts toward the longer wavelength region. Since Ge has a significant absorption at wavelengths up to about 2 μm, for comparison, the transmission spectra of Si(100) substrates coated with continuous Ge layers deposited at temperatures below 300 °C were measured (Fig. 3(b)). The measurements show that the continuous 40-nm thick Ge layer reduces the light transmission in the range of 1–2 μm less than the sample coated with SiGe particles obtained after the 7 nm Ge deposition. This indicates that the main effect of the decrease in the transmission of samples coated with SiGe particles after the Ge deposition in the amount of 20-60 nm can be associated with the excitation of EM Mie resonances which occur in dielectric particles.

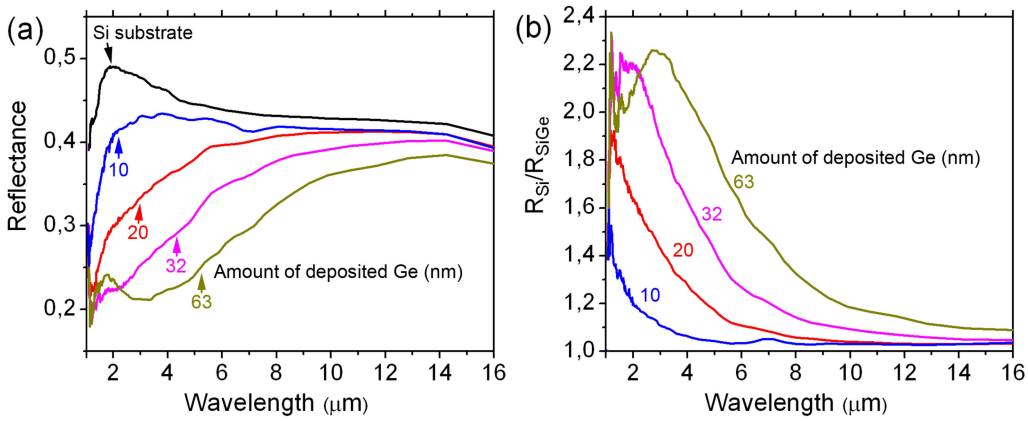

Fig. 4. (a) Reflectance spectra of the Si(100) substrate and the samples coated with SiGe particle arrays of prepared by the Ge deposition in the amounts of 10, 20, 32 and 63 nm on Si(100) at 850 °C, as marked. (b) Wavelength dependences of the ratio (R_{Si}/R_{SiGe}) of the reflectance spectra (shown in (a)) of Si(100) substrates coated with SiGe particles to the reflection spectrum of the uncoated Si(100) substrate. The deposited Ge amounts used for the SiGe particle formation are indicated at the corresponding curves.

The strongest decrease in the transmission under EM resonance conditions was observed for the samples obtained by the deposition of relatively large Ge amounts. The sample obtained by the 32 nm Ge deposition exhibits approximately a 25 times lower transmittance than the uncoated Si substrates (Fig. 3(c)). The transmission spectra show that, for the samples with the Ge coatings of 20 nm or less, the optical resonances in the corresponding SiGe particles are likely to be more pronounced at wavelengths less than 1 μm, at which Si substrates do not transmit EM radiation. For the samples with deposited Ge amounts of more than 32 nm, the transmission minimum is less deep, but significantly broader. This is, probably, due to a wider size distribution of SiGe particles in the corresponding coatings.

The reflectance spectra (R_{SiGe}) of the samples also exhibit a strong dependence on the SiGe particle size (Fig. 4(a)). The spectral dependences obtained by dividing the reflection spectrum of the Si substrate without particles (R_{Si}) by the reflection spectra of the Si substrate coated with the SiGe particles (R_{SiGe}) show that the presence of particles can reduce the EM reflection ~2.3 times at resonance wavelengths (Fig. 4(b)). In the reflection spectra, the resonance effects appear in a wider spectral range up to ~16 μm (Fig. 4(a)), compared to the transmission spectra in which they appear up to ~6 μm (Fig. 3(a)).

The absorption (1-R-T) by the samples coated with the SiGe particles at resonance wavelengths increases more than 70%, compared to a near-zero absorption by the Si substrates at wavelengths greater than 1.1 μm (Fig. 5). The enhanced absorption is observed in a wide wavelength range, which shifts toward longer wavelengths as the SiGe particle size increases.

The interaction of EM radiation with dielectric particles leads to the excitation of magnetic and electric resonances, among which dipole modes are the most intense and located in the long-wavelength region. Their position in the spectrum relative to each other depends on the particle shape. When the particle shape is described by two parameters (*h* and *d*), then the relative spectral position of the dipole modes can be characterized using such quantity as the particle aspect ratio [43], [44]. In our case, the SiGe particle shape is close to the sphere segment [34], [37], which is also described by the height and diameter at its base. For disk-shaped particles, it was shown that with increasing AR, the spectral position of the magnetic dipole mode shifts faster than the electric one [44]. At AR values in the range of 0.4–0.5, the spectral positions of the dipole modes coincide, and at larger AR values, the magnetic dipole mode wavelength is located in the region of longer wavelengths [44]. The SiGe particles grown at 850 °C are characterized by the AR values up to 0.6

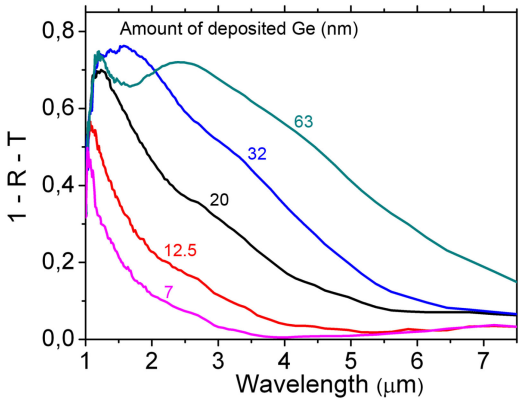

Fig. 5. Absorption spectra of the samples coated with SiGe particle arrays prepared by the Ge deposition in the amounts of 7, 12.5, 20, 32 and 63 nm on Si(100) at 850 °C. The deposited Ge amounts are marked at the corresponding curves.

[37], while typical AR values are in the range 0.4–0.5. This corresponds to the AR values at which the magnetic and electric dipole mode positions are close to each other.

The minimum in the transmission spectra of the substrates coated with dielectric particles is formed as a result of destructive interference between the incident EM field and the field of electric and magnetic dipole modes emitted by the particles [39], [40], [42]. The deepest minimum can appear at wavelengths at which electric and magnetic dipole modes equally contribute to the emitted EM field [16], [42], and when their resonant wavelength positions coincide. Such conditions take place for SiGe particles, in our case, due to their AR values. It is important to note that the similar AR values are quite common for particles that are naturally formed as a result of the liquid-state [48] and solid-state dewetting phenomenon [27], [32], [47].

There is a linear dependence

$$\lambda_{res} = \alpha \mathrm{nd} \tag{1}$$

between the wavelength λ_{res} of the magnetic dipole resonance and the particle diameter *d*, where α is the numerical coefficient depending on the shape of particles and their aspect ratio. For the spherical particles in the air, $\alpha \approx 1$ [11], while $\alpha \approx 1.2$ for the Si nanopillars with AR > 1 [51] and its value can be greater for the disk-like Ge particles with smaller AR [10] on Si substrates. Consider relation (1) with respect to our particles with the composition of $Si_{0.8}Ge_{0.2}$. The average lateral size of a particle at its base can be determined using the data for the area which the particle occupied on the substrate (Fig. 2) and assuming that the SiGe particles are shaped as a sphere segment. The corresponding distributions of particles as a function of their lateral size are shown in Fig. 6. The obtained distributions more pronounced reveal the bimodal size distribution for the particles obtained in the middle range (32 nm) of the deposited Ge amounts (Fig. 6(a)). The minima in the transmission spectra (Fig. 3(c)) are located in the wavelength region of $\sim$1.64 and 2.35 μm for the particles obtained by the Ge depositions with the thicknesses of 32 and 63 nm, respectively. For the particles of these samples, the average lateral size at their base is $\sim$1.05 (position of the larger peak in the bimodal distribution) and 1.5 μm, respectively (Fig. 6). Using pairs of these values and relation (1) with $\alpha = 1.2$, an effective refractive index $n_{eff} \approx 1.3$ can be obtained.

The refractive index (n_{SiGe}) of $Si_{0.8}Ge_{0.2}$ in the wavelength range of $\sim$2 μm is $n_{SiGe} \approx 3.6$ [52]. The n_{eff} value is significantly smaller than n_{SiGe}. Since relation (1) is well valid, the result obtained here means that the resonance modes of relatively small-sized particles give a significantly larger contribution in the optical properties than that of particles with larger sizes. This is confirmed by the estimation of the n_{eff} value using the minimum in the light transmission spectra of $\sim$1.64 μm (Fig. 3(a)) and the position (0.42 μm) of the first maximum of the bimodal particle size distribution (Fig. 6(a)) for the sample with the 32 nm Ge deposition, which gives $n_{eff} \approx 3.3$, that is, $n_{eff} \approx n_{SiGe}$.

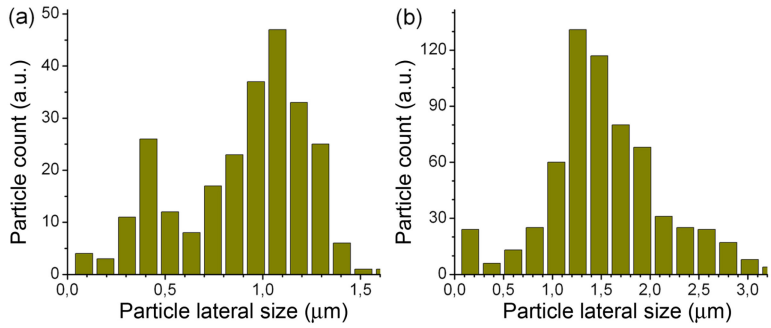

Fig. 6. The concentration of SiGe particles as a function of their average lateral size for the samples obtained by the Ge deposition in the amounts of (a) 32 and (b) 63 nm on Si(100) at 850 °C.

Thus, the relatively small particles produce the strong effect on the optical properties, despite their low concentration. At the same time, resonance modes in large particles cause a significant decrease in the transmission and reflection in a wide wavelength range up to 7 μm and more (Fig. 3 and 4).

The compact particle formation during the agglomeration of continuous layers on a non-wettable substrate depends on their thickness and crystal structure. Crystalline and polycrystalline layers are thermally more stable than amorphous ones. The particles formation on SiO_2 requires temperatures $\geq$800 °C for the crystalline Si [20], [44], [45], SiGe [55]–[57] and Ge [31], [48] layers, and $\geq$700 °C for the amorphous Ge layers, depending on the thickness [32]. In the similar temperature range ($\geq$750 °C), the SiGe particle formation occurs during the Ge deposition on the bare Si(100) [34], [37] and Si(111) [33], [35] substrates. However, there are significant differences between the arrays of particles formed on the SiO_2 and Si surfaces. In the case of Si on SiO_2, the maximum possible lateral size of compact particles is up to 500 nm [29], [53], whereas the lateral size of compact SiGe particles on Si(100) reaches 3 μm [37]. Moreover, the SiGe particles on Si(100) have a higher concentration and aspect ratio. These differences characterize the SiGe particles on Si(100), obtained due to the self-organized agglomeration, as more effective in their influence on the optical properties.

The observed broadband minima in the reflectance and transmission spectra are associated with the broad particle size distribution. Another reason for the broadening of the resonance minima is due to the influence of the substrate. Spinelli et al. [50], by means of calculations, showed that the resonance minima from a Si cylinder lying directly on a high-index substrate are wider than from the same Si cylinder surrounded by the air. This is due to the propagation of a significant part of the resonant EM waves into the substrate, which is confirmed by the theoretical calculations [58] and Raman spectroscopy data that reveal the Raman signal amplification from the Si substrate areas located under SiGe particles [59], [60]. It was shown for particles of the same size that, in a narrow spectral range, the dielectric particle array is more efficient as an antireflection coating than the metal particles array [61]. A significant expansion of the spectral range due to two factors, namely, the influence of a high-index substrate and a wide particle size distribution, makes the dielectric particle array to be more efficient as antireflective coatings in a wide spectral range in comparison with coatings made of metal particles. From the fabrication viewpoint, the simplest are antireflection coatings made of continuous transparent layers of certain thicknesses which suppress the back-reflection due to the interference of light reflected from interlayer boundaries. This interference forms relatively narrowband antireflection coatings. Moreover, the band spectral position depends on the light incidence angle. The interference associated with the participation of magnetic and electrical resonance waves from arrays of compact dielectric particles does not have such limiting spectral characteristics. Thus, dielectric SiGe particle arrays can be used as antireflection coatings to increase the efficiency of photodetectors, solar cells and photoluminescent radiations.

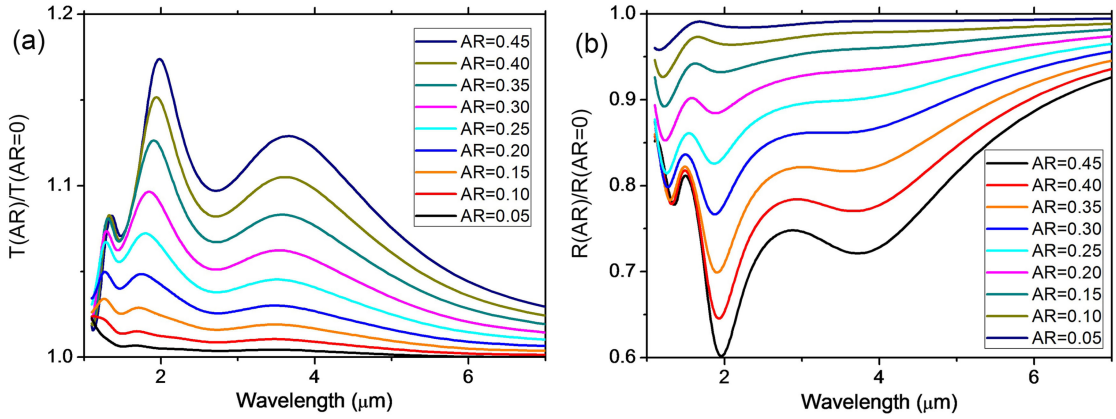

Fig. 7. Normalized intensity of (a) transmitted and (b) reflected EM waves for the $Si_{0.8}Ge_{0.2}$ particle on the Si substrate for different AR values at fixed $d = 1.0$ μm.

3.3 Numerical Simulations

The numerical simulation of the SiGe particles on a Si substrate was performed using the finite difference time domain (FDTD) method through the commercial software package FullWave by RSoft-SYNOPSYS [62]. The refractive index of Si_xGe_{1-x} was obtained according to the generalized Vegard's law by the linear interpolation from *n* for Si to *n* for Ge using their data known from the literature. The modeled particle is shaped as a sphere segment with $d = 1$ mm and AR in the range from 0.05 to 0.45 and $x = 0.8$.

The numerical simulations show that the $Si_{0.8}Ge_{0.2}$ particle on Si substrates has such optical properties that are very different from the optical properties of the Si sphere on silica [11]. In our case the structure of the $Si_{0.8}Ge_{0.2}$ particle on the Si substrate has a very small (13%) difference in *n* at their interface. As a result, this structure has a very low Q-factor. An incident EM wave can excite the SiGe particle, but it exhibits the behavior of a weak resonator which has broadband excitations at different wavelengths. This is the main difference from the excitation of the Si sphere in the air or on silica [11], at which the contribution of different resonance modes can be well distinguished at each wavelength.

To reveal the optical properties of the $Si_{0.8}Ge_{0.2}$ particle on Si substrates by the numerical simulation, we excited the structure with a Gaussian EM beam, which is incident on it in the direction normal to the substrate surface. The incident wave that contains the broad spectrum excites the $Si_{0.8}Ge_{0.2}$ particle and produces the scattering field having the local maxima corresponding to the excitation of electric and magnetic moments described by eclectic (E_z) and magnetic (H_z) field components, respectively. The calculated intensity dependences of reflected and transmitted EM waves are presented on Fig. 7.

To obtain the scattering field generated only by the $Si_{0.8}Ge_{0.2}$ particle on the Si substrate, the following procedure was used. We calculated the total scattering fields separately for two cases: for the bare Si substrate and for the Si substrate with the $Si_{0.8}Ge_{0.2}$ particle. Then we subtracted the calculation result for the first case from the calculation result for the second case. This procedure is suggested to allow obtaining the reflected and transmitted spectra, and the EM resonance fields generated by only the $Si_{0.8}Ge_{0.2}$ particle, which is shown in Figs. 8 and 9, respectively. As expected, the spatial distribution of the Ez and Hz components of the EM field corresponds to dipole-type excitations [Fig. 9(a), (b)], and their distribution in the *x* and *y* planes reflects the electromagnetic field leakage into the substrate, as was observed for similar structures using Raman spectroscopy [59], [60].

It is shown in Fig. 8 that the peaks of the strong resonant interaction between the EM radiation and the $Si_{0.8}Ge_{0.2}$ particles on Si substrates lie at the wavelengths of $\sim$2 and 3.5 μm for the particles with the diameter of 1 μm. This gives $n_{eff} \approx$ 2 and 3.5, respectively, according to relation

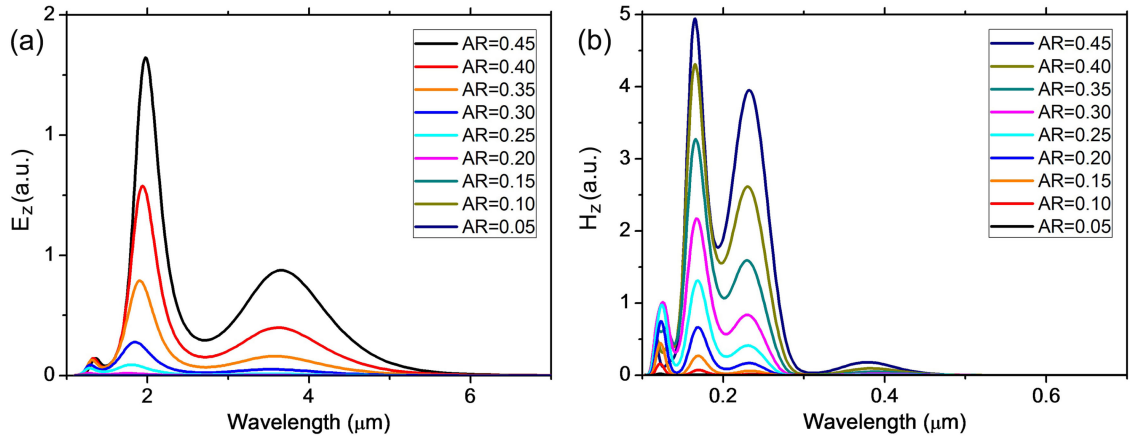

Fig. 8. Amplitude of the scattering (a) E_z and (b) H_z components of the EM field by the $Si_{0.8}Ge_{0.2}$ particle on the Si substrate; it was measured near the substrate surface, but far from the particle.

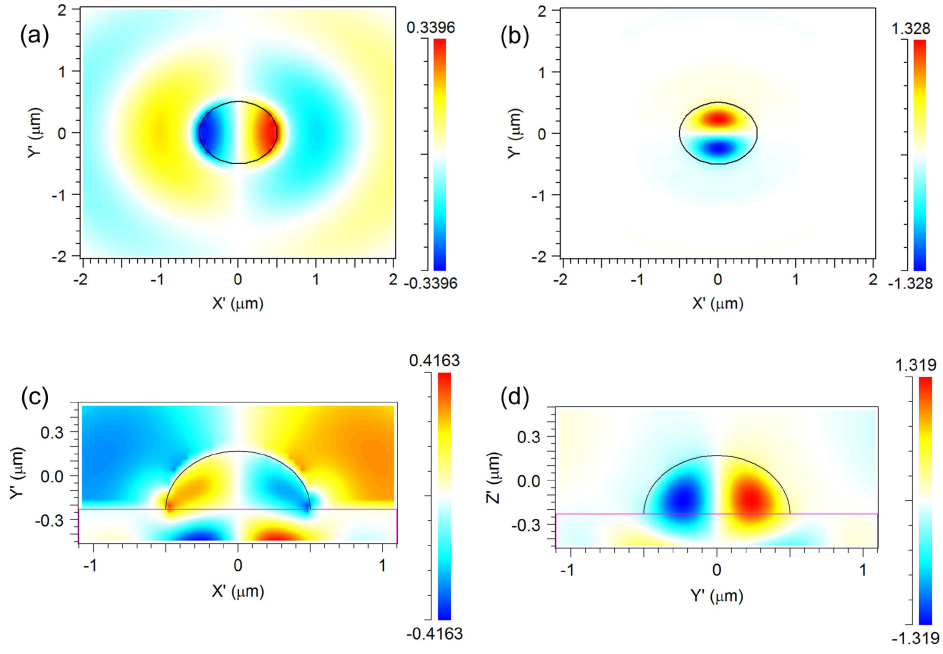

Fig. 9. Spatial distribution of the real part of (a, c) E_z and (b, d) H_z components of the EM field scattered by the $Si_{0.8}Ge_{0.2}$ particle: (a, b) Z-cut, (c) Y-cut and (d) X-cut. The calculation was performed for $\lambda = 2.32$ μm, $d = 1.0$ μm and AR $= 0.4$. The scales show the relative values of the amplitudes for the (a, c) E_z and (b, d) H_z components in arbitrary units.

(1). Thus, the results of numerical simulation are in a good agreement with the experimental data and show that the structures studied by us are characterized by several resonance peaks resulting in the broadband interaction.

The numerical simulation shows that the spectral position of the maxima and minima in the obtained spectra is determined only by the particle diameter and, practically, does not depend on the AR value. Such dependence on the AR value is in agreement with the experimental data obtained for the dependences on AR for the Ge particles of a disk-like shape on Si substrates [19]. The second agreement with the experimental data is the presence of a strong dependence of the

maxima and minima amplitudes of the obtained spectra on the AR value [19]. The particles with small AR values exhibit weakly pronounced resonance properties, since the influence of a low Q-factor of the corresponding structures is more significant. Thus, the results of the experiment and numerical simulations show that, despite the low Q-factor, the structures exhibit strong EM resonance effects in the transmission and reflection spectra at relatively large AR values . As for the dewetting phenomena used here for the particle fabrication, it provides the formation of particles with sufficiently high AR values at which the small difference in n at the interface has a reduced effect on the resonance excitation.

4. Conclusion

The transmission and reflection spectra were obtained for Si(100) substrates coated with submicron- and micron-sized SiGe particles which were formed using the dewetting phenomenon. The spectra contain deep minima, in which the transmission and reflection can decrease more than 20 and 2 times, respectively, in comparison with the sample not coated with the particles. These minima are associated with the destructive interference of the incident EM field and the field of electric and magnetic dipole resonances generated in the dielectric SiGe particles. The estimates of the refractive index of SiGe particles based on the values of the resonance wavelengths and the position of the maxima in the particle size distributions showed that resonances in smaller particles make a stronger contribution to the destructive interference, while the contribution of large particles is distributed over a wide wavelength range up to 7 μm and more. The numerical simulation using the FDTD method confirms that the EM field generates strong EM resonance excitations in the SiGe particles with relatively large AR values. These resonances have a low Q-factor due to the small reflective index contrast at the particle/substrate interface, causing the resonance EM field leakage into the substrate. The obtained results show that strong antireflection properties become broadband for the coatings consisting of dielectric particles with a hemispherical-like shape and broad size distribution. Particles with similar shapes and size distributions are commonly formed by the dewetting phenomenon.

Acknowledgment

The author would like to express his gratitude to Prof. V.A. Volodin for his help in the optical measurements.

References

[1] R. Stanley, "Plasmonics in the mid-infrared," *Nature Photon.*, vol. 6, pp. 409–411, 2012.
[2] C. L. Tan and H. Mohseni, "Emerging technologies for high performance infrared detectors," *Nanophotonics*, vol. 7, pp. 169–197, 2018.
[3] J. Tong, F. Suo, J. Ma, L. Tobing, L. Qian, and D. Zhang, "Surface plasmon enhanced infrared photodetection," *Opto-Electron. Adv.*, vol. 2, 2019, Art. no. 180026.
[4] A. I. Yakimov, V. V. Kirienko, A. A. Bloshkin, A. V. Dvurechenskii, and D. E. Utkin, "Quantum dot based mid-infrared photodetector enhanced by a hybrid metal-dielectric optical antenna," *J. Phys. D: Appl. Phys.*, vol. 53, 2020, Art. no. 335105.
[5] C.-C. Chang *et al.*, "A surface plasmon enhanced infrared photodetector based on inas quantum dots," *Nano Lett.*, vol. 10, pp. 1704–1709, 2010.
[6] A. I. Yakimov, V. V. Kirienko, A. A. Bloshkin, A. V. Dvurechenskii, and D. E. Utkin, "Mid-infrared optical resonances in quantum dot photodetectors coupled with metallic gratings with different aperture diameters," *Curr. Appl. Phys.*, vol. 20, pp. 877–882, 2020.
[7] S. Savoia *et al.*, "Surface sensitivity of rayleigh anomalies in metallic nanogratings," *Opt. Exp.*, vol. 21, no. 20, pp. 23531–23542, 2013.
[8] N. Sardana *et al.*, "Localized surface plasmon resonance in the IR regime," *Opt. Exp.*, vol. 24, no. 1, pp. 254–261, 2016.
[9] R. Kumar and S. A. Ramakrishna, "Enhanced infra-red transmission through subwavelength hole arrays in a thin gold film mounted with dielectric micro-domes," *J. Phys. D: Appl. Phys.*, vol. 51, 2018, Art. no. 165104.
[10] A. I. Kuznetsov, A. E. Miroshnichenko, Y. H. Fu, J. B. Zhang, and B. Luk'yanchuk, "Magnetic light," *Sci. Rep.*, vol. 2, 2012, Art. no. 492.

[11] A. B. Evlyukhin *et al.*, "Demonstration of magnetic dipole resonances of dielectric nanospheres in the visible region," *Nano Lett.*, vol. 12, no. 7, pp. 3749–3755, 2012.
[12] K. Koshelev, G. Favraud, A. Bogdanov, Y. Kivshar, and A. Fratalocchi, "Nonradiating photonics with resonant dielectric nanostructures," *Nanophotonics*, vol. 8, no. 5, pp. 725–745, 2019.
[13] C. Li *et al.*, "Dielectric metasurfaces: From wavefront shaping to quantum platforms," *Prog. Surf. Sci.*, vol. 95, no. 2, 2020, Art. no.100584.
[14] J. A. Schuller and M. L. Brongersma, "General properties of dielectric optical antennas," *Opt. Exp.*, vol. 17, no. 26, pp. 24084–24095, 2009.
[15] Z. Wang *et al.*, "High order fano resonances and giant magnetic fields in dielectric microspheres," *Sci. Rep.*, vol. 9, 2019, Art. no. 20293.
[16] J. Tian, Q. Li, P. A. Belov, R. K. Sinha, W. Qian, and M. Qiu, "HighQ all-dielectric metasurface: Super and suppressed optical absorption," *ACS Photon.*, vol. 7, no. 6, ppp. 1436−1443, 2020.
[17] M. V. Stepikhova *et al.*, "Light emission from Ge(Si)/SOI self-assembled nanoislands embedded in photonic crystal slabs of various periods with and without cavities," *Semicond. Sci. Technol.*, vol. 34, no. 2, 2019, Art. no. 024003.
[18] T. D. Gupta *et al.*, "Self-assembly of nanostructured glass metasurfaces via templated fluid instabilities," *Nature Nanotechnol.*, vol. 14, pp. 320–327, 2019.
[19] D. E. Utkin, K. V. Anikin, S. L. Veber, and A. A. Shklyaev, "Dependence of light reflection of germanium Mie nanoresonators on their aspect ratio," *Opt. Mater.*, vol. 109, 2020, Art. no. 110466.
[20] P. Molet *et al.*, "Large area metasurfaces made with spherical silicon resonators," *Nanophotonics*, vol. 9, no. 4, pp. 943–951, 2020.
[21] U. Zywietz, A. Evlyukhin, C. Reinhardt, and B. N. Chichkov, "Laser printing of silicon nanoparticles with resonant optical electric and magnetic responses," *Nature Commun.*, vol. 5, 2014, Art. no. 3402.
[22] J. Berzins *et al.*, "Direct and high-throughput fabrication of mie-resonant metasurfaces via single-pulse laser interference," *ACS Nano*, vol. 14, no. 5, pp. 6138−6149, 2020.
[23] Y. Ono, M. Nagase, M. Tabe, and Y. Takahashi, "Thermal agglomeration of thin single crystal Si on SiO_2 in vacuum," *Jpn. J. Appl. Phys.*, vol. 34, pp. 1728–1735, 1995.
[24] Y. Wakayama, T. Tagami, and S. Tanaka, "Three-dimensional islands of Si and Ge formed on SiO_2 through crystallization and agglomeration from amorphous thin films," *Thin Solid Films*, vol. 350, pp. 300–307, 1999.
[25] R. Nuryadi, Y. Ishikawa, and M. Tabe, "Formation and ordering of self-assembled Si islands by ultrahigh vacuum annealing of ultrathin bonded silicon-on-insulator structure," *Appl. Surf. Sci.*, vol. 159-160, pp. 121–126, 2000.
[26] A. A. Shklyaev and M. Ichikawa, "Three-dimensional Si islands on Si(001) surfaces," *Phys. Rev. B*, vol. 65, no. 4, 2002, Art. no. 045307.
[27] A. A. Shklyaev and M. Ichikawa, "Extremely dense arrays of germanium and silicon nanostructures," *Phys.-Usp,* vol. 51, no. 2, pp. 133–161, 2008.
[28] Y. Fan, R. Nuryadi, Z. A. Burhanudin, and M. Tabe, "Thermal agglomeration of ultrathin silicon-on-insulator layers: Crystalline orientation dependence," *Jpn. J. Appl. Phys.*, vol. 47, no 3R, pp. 1461–1464, 2008.
[29] M. Abbarchi *et al.,* "Wafer scale formation of monocrystalline silicon-based mie resonators via silicon-on-insulator dewetting," *ACS Nano*, vol. 8, no. 11, pp. 11181–11190, 2014.
[30] A. A. Shklyaev, M. Shibata, and M. Ichikawa, "High-density ultrasmall epitaxial Ge islands on Si(111) surfaces with a SiO_2 coverage," *Phys. Rev. B*, vol. 62, no. 3, pp. 1540–1543, 2000.
[31] F. Cheynis, F. Leroy, T. Passanante, and P. Müller, "Agglomeration dynamics of germanium islands on a silicon oxide substrate: A grazing incidence small-angle X-ray scattering study," *Appl. Phys. Lett.*, vol. 102, no. 16, 2013, Art. no. 161603.
[32] A. A. Shklyaev and A. V. Latyshev, "Dewetting behavior of ge layers on SiO_2 under annealing," *Sci. Rep.*, vol. 10, 2020, Atr. no. 13759.
[33] A. Shklyaev, L. Bolotov, V. Poborchii, and T. Tada, "Properties of three-dimensional structures prepared by Ge dewetting from Si(111) at high temperatures," *J. Appl. Phys.*, vol. 117, no. 20, 2015, Art. no. 205303.
[34] A. A. Shklyaev and A. E. Budazhapova, "Ge deposition on Si(100) in the conditions close o dynamic equilibrium between islands growth and their decay," *Appl. Surf. Sci.*, vol. 360, Part B, pp. 1023–1029, 2016.
[35] A. A. Shklyaev and K. E. Ponomarev, "Strain-induced Ge segregation on Si at high temperatures," *J. Cryst. Growth*, vol. 413, pp. 94–99, 2015.
[36] A. A. Shklyaev, V. A. Volodin, M. Stoffel, H. Rinnert, and M. Vergnat, "Raman and photoluminescence spectroscopy of sige layer evolution on Si(100) induced by dewetting," *J. Appl. Phys.*, vol. 123, no. 1, 2018, Art. no. 015304.
[37] A. A. Shklyaev and A. E. Budazhapova, "Submicron- and micron-sized sige island formation on Si(100) by dewetting," *Thin Solid Films*, vol. 642, pp. 345–351, 2017.
[38] M. Kerker, D.-S. Wang, and C. L. Giles, "Electromagnetic scattering by magnetic spheres," *J. Opt. Soc. Amer.*, vol. 73, no. 6, pp. 765–767, 1983.
[39] R. Gomez-Medina *et al.*, "Electric and magnetic dipolar response of germanium nanospheres: Interference effects, scattering anisotropy, and optical forces," *J. Nanophotonics*, vol. 5, no. 1, 2011, Art. no. 053512.
[40] Y. H. Fu, A. I. Kuznetsov, A. E. Miroshnichenko, Y. F. Yu, and B. Lukyanchuk, "Directional visible light scattering by silicon nanoparticles," *Nature Commun.*, vol. 4, 2013, Art. no. 1527.
[41] B. S. Luk'yanchuk, N. V. Voshchinnikov, R. Paniagua-Dominguez, and A. I. Kuznetsov, "Optimum forward light scattering by spherical and spheroidal dielectric nanoparticles with high refractive index," *ACS Photon.*, vol. 2, no. 7, pp. 993–999, 2015.
[42] J. Tian, H. Luo, Q. Li, X. Pei, K. Du, and M. Qiu, "Near-infrared super-absorbing all-dielectric metasurface based on single-layer germanium nanostructures," *Laser Photon. Rev.*, vol. 12, no. 9, 2018, Art. no. 1800076.
[43] I. Staude *et al.*, "Tailoring directional scattering through magnetic and electric resonances in subwavelength silicon nanodisks," *ACS Nano*, vol. 7, no. 9, pp. 7824–7832, 2013.
[44] P. Moitra, B. A. Slovick, Z. G. Yu, S. Krishnamurthy, and J. Valentine, "Experimental demonstration of a broadband all-dielectric metamaterial perfect reflector," *Appl. Phys. Lett.*, vol. 104, no. 17, 2014, Art. no. 171102.

[45] M. Decker *et al.*, "High-efficiency dielectric huygens' surfaces," *Adv. Opt. Mater.*, vol. 3, no. 6, pp. 813–820, 2015.
[46] P. Molet *et al.*, "Large area metasurfaces made with spherical silicon resonators," *Nanophotonics*, vol. 9, no. 4, pp. 943–951, 2020.
[47] M. Naffouti *et al.*, "Fabrication of poly-crystalline Si-based Mie resonators via amorphous Si on SiO_2 dewetting," *Nanoscale*, vol. 8, no. 5, pp. 2844–2849, 2016.
[48] C. Dabard, A. A. Shklyaev, V. A. Armbrister, and A. L. Aseev, "Effect of deposition conditions on the thermal stability of Ge layers on SiO_2 and their dewetting behavior," *Thin Solid Films*, vol. 693, 2020, Art. no. 137681.
[49] A. A. Shklyaev and A. E. Budazhapova, "Critical conditions for sige island formation during Ge deposition on Si(100) at high temperatures," *Mater. Sci. Semicond. Proc.*, vol. 57, pp. 18–23, 2017.
[50] P. Spinelli, M. A. Verschuuren, and A. Polman, "Broadband omnidirectional antireflection coating based on subwavelength surface mie resonators," *Nature Commun.*, vol. 3, 2012, Art. no. 692.
[51] F. J. Bezares *et al.*, "Mie resonance-enhanced light absorption in periodic silicon nanopillar arrays," *Opt. Exp.*, vol. 21, no. 23, pp. 27587–27601, 2013.
[52] P. Barritault, M. Brun, P. Labeye, O. Lartigue, J.-M. Hartmann, and S. Nicoletti, "Mlines characterization of the refractive index profile of sige gradient waveguides at 2.15 μm," *Opt. Exp.*, vol. 21, no. 9, pp. 11506–11515, 2013.
[53] R. Nuryadi, Y. Ishikawa, Y. Ono, and M. Tabe, "Thermal agglomeration of single-crystalline Si layer on buried SiO_2 in ultrahigh vacuum," *J. Vac. Sci. Technol. B*, vol. 20, no. 1, pp. 167–172, 2002.
[54] D. T. Danielson, D. K. Sparacin, J. Michel, and L. C. Kimerling, "Surface-energy-driven dewetting theory of silicon-on-insulator agglomeration," *J. Appl. Phys.*, vol. 100, no. 8, 2006, Art. no. 083507.
[55] E. Sutter and P. Sutter, "Assembly of Ge nanocrystals on SiO_2 via a stress-induced dewetting process," *Nanotechnology*, vol. 17, no. 15, pp. 3724–3727, 2006.
[56] E. Mitsai *et al.*, "$Si_{1-x}Ge_x$ nanoantennas with a tailored raman response and light-to-heat conversion for advanced sensing applications," *Nanoscale*, vol. 11, no. 24, pp. 11634–11641, 2019.
[57] V. Poborchii *et al.*, "Raman microscopy and infrared optical properties of sige mie resonators formed on SiO_2 via Ge condensation and solid state dewetting," *Nanotechnology*, vol. 31, no. 19, 2020, Art. no. 195602.
[58] J. Van de Groep and A. Polman, "Designing dielectric resonators on substrates: Combining magnetic and electric resonances," *Opt. Exp.*, vol. 21, no. 22, pp. 26285–26302, 2013.
[59] V. Poborchii, A. Shklyaev, L. Bolotov, N. Uchida, T. Tada, and Z. N. Utegulov, "Photonic metasurface made of array of lens-like sige mie resonators formed on (100) Si substrate via dewetting," *Appl. Phys. Exp.*, vol. 10, no. 12, 2017, Art. no. 125501.
[60] V. Poborchii, A. Shklyaev, L. Bolotov, and N. Uchida, "Nanoscale characterization of photonic metasurface made of lens-like sige Mie-resonators formed on Si(100) substrate," *J. Appl. Phys.*, vol. 126, no. 12, 2019, Art. no. 123102.
[61] K. V. Baryshnikova, M. I. Petrov, V. E. Babicheva, and P. A. Belov, "Plasmonic and silicon spherical nanoparticle antireflective coatings," *Sci. Rep.*, vol. 6, 2016, Art. no. 22136.
[62] Synopsys, FDTD Simulation Software–FullWAVE: RSoft Products (version 2020.09-1). Synopsys, Mountain View, CA, USA, 2020. [Online]. Available: https://www.synopsys.com/photonic-solutions/rsoft-photonic-device-tools/passive-device-fullwave.html.